Asbestiform riebeckite (crocidolite) dissolution in the presence of Fe chelators: Implications for mineral-induced disease

ANDREW J. WERNER,* MICHAEL F. HOCHELLA, JR.

Department of Geological Sciences, Virginia Polytechnic Institute and State University,
Blacksburg, Virginia 24061, U.S.A.

GEORGE D. GUTHRIE, JR.

Geology and Geochemistry Group, EES-1, Los Alamos National Laboratory,
Los Alamos, New Mexico 87545, U.S.A.

JEANNE A. HARDY,** ANN E. AUST

Department of Chemistry and Biochemistry, Utah State University,
Logan, Utah 84332, U.S.A.

J. DONALD RIMSTIDT

Department of Geological Sciences, Virginia Polytechnic Institute and State University,
Blacksburg, Virginia 24061, U.S.A.

ABSTRACT

X-ray photoelectron spectroscopy (XPS) and solution chemistry were used to monitor the changes in surface composition of crocidolite fibers in a 50 mM NaCl solution at pH = 7.5 and 22 °C in the presence of several Fe chelators (citrate, EDTA, or desferrioxamine) for up to 30 d. The data show that the introduction of Fe chelators dramatically increases the rate at which Fe is released from the surface in comparison with a control group to which no chelators were added. In particular, XPS shows that Fe^{3+} is more effectively removed in the presence of the chelators even though it is highly insoluble in aqueous solutions at near neutral pH. This suggests that Fe chelators can alter the dissolution mechanism of amphiboles from the process that dominates in NaCl solutions. This change in dissolution mechanism (particularly the enhanced rate of Fe release) is an important consideration for models of mineral-induced pathogenesis that rely on oxidation and reduction processes.

Efforts were made to estimate the Fe-release lifetimes of crocidolite fibers under the conditions of our experiments to guide the assessment of the biodurability of these fibers in human lung tissue. Our results suggest that crocidolite fibers may persist for several years, releasing Fe to lung fluids during this time. This estimated lifetime is longer than that previously estimated for chrysotile fibers and is consistent with the lifetimes previously observed in asbestos mineral lung-burden studies.

INTRODUCTION

Asbestiform minerals were used widely in the past in various industrial and nonindustrial applications because of their fibrous shape, high tensile strength, flexibility, long-term durability, and fire resistance. The most commonly used asbestos minerals were the 1:1 sheet silicate chrysotile $[Mg_3Si_2O_5(OH)_4]$ and the amphibole crocidolite $[Na_2Fe_2^{3+}(Fe^{2+},Mg^{2+})_3Si_8O_{22}(OH)_2]$, the fibrous variety of riebeckite. It is now known that asbestos minerals have the ability to induce lung diseases such as asbestosis (scarring of lung tissue, which results in a significant decrease in blood oxygenation efficiency), mesothelioma (a malignant tumor of the pleura, the membrane lining the cavities containing the lungs), and lung cancer, although exactly which mineral is responsible for inducing a particular disease is often debated (e.g., Wagner et al., 1960; Craighead et al., 1982; Wagner, 1991; Guthrie and Mossman, 1993). Unfortunately, the processes by which certain fibrous minerals induce diseases are not yet known, although many studies have investigated this problem (see Guthrie and Mossman, 1993, and references therein). Stanton et al. (1981) reported a positive correlation between the number of fibers, as well as their dimension, and the sample's ability to induce cancer following direct application to the pleural surface of rats. They concluded that fibers with a diameter <0.25 μm and a length >8

μm were the most carcinogenic. This is referred to as the Stanton hypothesis. The Stanton hypothesis contributed significantly to the current restrictive regulations and guidelines on asbestos use and exposure in the U.S. (Vu, 1993). In a recent paper, Nolan and Langer (1993) reviewed what are now recognized as major limitations in the Stanton studies; they stated that, although the fiber dimension vs. pathogenicity (disease generation) relationship may hold true in some instances, the overall findings of Stanton et al. (1981) are inconclusive insofar as their relevance to human disease. Besides the fibrous nature of certain minerals, there are several other mineralogical properties that can potentially control their deleterious effects on our respiratory systems. For example, the ability of physiological fluids to leach constituent metals from mineral fibers has been studied in test animals (e.g., Morgan et al., 1971), in human lungs (e.g., Jaurand et al., 1977), and in vitro (e.g., Hart et al., 1980). Related to this, fiber durability (i.e., the lifetime of a fiber on the basis of its dissolution rate) in lung tissue appears to play an important role in pathogenesis (e.g., McDonald and McDonald, 1986a, 1986b). Surface characteristics of asbestos fibers, such as charge, composition, structure, and microtopography may also influence fiber reaction in and perturbation of respiratory systems (e.g., Hochella, 1993). Even mechanical properties (stiffness, fragmenting characteristics, etc.) may be important as fibers translocate from the respiratory tract to the pleura.

A major implication of most of the studies mentioned above is that there is an important need for an understanding of how minerals chemically interact with physiological fluids. This is likely to be a necessary component of any integrated model of mineral-induced pathogenesis. In this study, we investigated the surface chemistry of crocidolite fibers and particularly the surface chemistry of Fe on these fibers. We specifically chose crocidolite for our work because it is clear from epidemiological studies that crocidolite is far more pathogenic in humans than chrysotile for the induction of mesothelioma (e.g., Wagner et al., 1960; McDonald and McDonald, 1986a). Crocidolite can also induce lung cancer and asbestosis (e.g., McDonald and McDonald, 1986b; McDonald, 1990). Furthermore, the surface chemistry of Fe on these fibers is of special interest to us because of previous work on the generation of O radicals by asbestos (see the extensive review by Kamp et al., 1992). In particular, Weitzman and Graceffa (1984), Goodglick and Kane (1986), Kennedy et al. (1989), Aust and Lund (1990, 1991), Lund and Aust (1990, 1992), Gulumian et al. (1993), Ghio et al. (1994), Lund et al. (1994), Chao and Aust (1993), and Hardy and Aust (1995) have suggested that OH radicals (·OH) may be important in mineral-induced disease. Although extremely short-lived, they have the ability to fragment DNA. For example, Aust and coworkers studied the release of Fe from crocidolite in vitro and reported a link between this and DNA single-strand breaks (SSBs) (Aust and Lund, 1990, 1991; Lund and Aust, 1992). Measurements of DNA SSBs is one way of as-

sessing how an agent interacts with DNA, and SSBs themselves may be an important component of the disease process.

One mechanism for the generation of ·OH, created by reactions involving Fe either on the surface of or released from amphibole asbestos minerals, is shown in the following series of reactions referred to as the modified, Fe-catalyzed Haber-Weiss reactions (e.g., Zalma et al., 1987a, 1987b; Hardy and Aust, 1995):

$$\text{Reductant}^{(n)} + Fe^{3+} \rightarrow \text{reductant}^{(n+1)} + Fe^{2+} \quad (1)$$

$$Fe^{2+} + O_2 \rightarrow Fe^{3+} + O_2\text{-} \quad (2)$$

$$HO_2^. + O_2\text{-} + H^+ \rightarrow O_2 + H_2O_2 \quad (3)$$

$$Fe^{2+} + H_2O_2 \rightarrow Fe^{3+} + OH^- + \text{·OH}$$
$$\text{(Fenton reaction).} \quad (4)$$
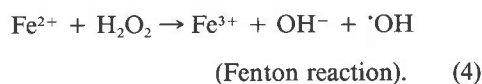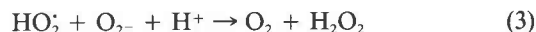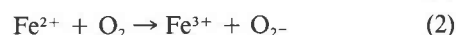
Because Fe^{3+} is so immobile under near neutral conditions in aqueous solutions (e.g., Baes and Mesmer, 1976), leaching experiments have been conducted in the presence of Fe chelators (Aust and Lund, 1990, 1991; Lund and Aust, 1992). It is well established that chelators can promote mineral dissolution by interacting directly with metals on mineral surfaces (e.g., Hering and Stumm, 1990; Schindler, 1990; Stumm, 1992; and many references therein). Because chelators are present in physiological fluids, they also may be important in the disease process in their ability to extract Fe efficiently from fiber surfaces (Lund and Aust, 1990).

There is much interest in Fe in studies dealing with mineral-induced disease despite the fact that hematite, for example, has negligible biochemical reactivity and erionite, an Fe-free zeolite, has high reactivity. This may suggest that there are several pathways by which various minerals induce the same disease in humans. It is also a reminder that there are probably several factors that combine to result in the pathogenicity of minerals. Hematite, as a nonfibrous mineral but one with very low solubility, is much more likely to be physically cleared from the lung by means of the mucociliary escalator than a fibrous mineral (e.g., Lehnert, 1993). On the other hand, Fe sorbed on the surface of erionite in vitro has been shown to produce DNA SSBs, whereas erionite without sorbed Fe does not (Eborn and Aust, 1995; Hardy and Aust, 1995).

Several previous studies on the pathogenic role of crocidolite have focused primarily on Fe-release rate, OH radical generation, and DNA damage. As alluded to above, our work was specifically designed to begin to study the surface chemistry of crocidolite, especially that pertaining to both Fe^{2+} and Fe^{3+}, as it dissolves under conditions similar to those of a human lung. We used X-ray photoelectron spectroscopy (XPS) and solution analysis to track the changes in surface chemistry and the contacting solutions over a 30 d period. Scanning electron microscopy (SEM) was also used to look for any dissolution or depositional features on these fibers after treat-

ment. In addition, because of the potential importance of chelators in the disease process as described above, three well-known Fe chelators were chosen for this study, including ethylenediaminetetraacetic acid (EDTA), desferrioxamine, and citrate. Although citrate is the only one of the three found in the body, EDTA and desferrioxamine were also used because they are very effective Fe chelators and may have application in fiber-surface modification relevant to reducing toxicity of fibers (e.g., Brown et al., 1990; Klockars et al., 1990; Gulumian et al., 1993). Ultimately, the results of this study combined with previous work may help lead to a model for mineral-induced pathogenesis that more specifically includes the involvement of reactions at the mineral-fluid interface.

MATERIALS AND METHODS

Samples and reagents

Crocidolite samples were obtained from Richard Griesemer (National Institute of Environmental Health Sciences, National Toxicology Program, Research Triangle Park, North Carolina). Campbell et al. (1980) report median fiber size of roughly 15.0×0.25 μm. The bulk composition was determined by wet chemical methods (Campbell et al., 1980) and is as follows (converted to atomic percent for use with XPS data; see Eq. 5): Si 18.6%, Fe^{2+} 5.9%, Fe^{3+} 5.4%, Mg 2.1%, and Na 3.3%.

Two of the Fe chelators (sodium citrate and disodium salt of EDTA) were obtained from Mallinckrodt, Inc. (Paris, Kentucky). Deferoxamine mesylate USP (desferrioxamine-B) was obtained from CIBA (Summit, New Jersey). Stability constants for these chelators are available in Martell and Smith (1974, 1977). In every case, the stability constant for chelated Fe^{3+} is higher than that for chelated Fe^{2+}. However, it is not clear how this may affect crocidolite dissolution.

Sample treatment

Crocidolite (1 mg/mL) was reacted in a 50 mM NaCl solution in glass vials in air at a pH of 7.5 and room temperature ($\sim$22 °C). Although physiological saline is approximately three times this concentration, we chose 50 mM for direct comparison with previous studies (see Introduction). The pH was initially adjusted to 7.5 using NaOH. The volume of the solution was approximately 50 mL. The solutions were reacted for time periods of 1, 24, and 720 h (30 d) in 1 mM citrate, EDTA, or desferrioxamine-B. Millimolar chelator concentrations were used to approximate the concentrations of citrate and other organic acids found under actual physiological conditions. All experiments were performed in triplicate. One control group was analyzed for each time period without a chelator added. The 30 d experiments were resuspended in fresh chelator solutions on the first and seventh days, and the pH was readjusted to 7.5. The resuspension protocol was used to refresh the chelators, which are subject to unwanted polymerization and potential OH radical destruction. This also afforded a reasonable method of pH

control. The pH adjustment was performed only during resuspension to keep the solutions sterile more easily. Buffers were not used because they could bind to fibers or chelate Fe themselves (Lund and Aust, 1990). Each sample was placed on a wrist-action shaker for the first hour of reaction at each stage, and each was kept in the dark to avoid photochemical reduction of Fe^{3+} by the chelators (Chao and Aust, 1993). After the reaction period, the suspension was transferred to 50 mL conical bottom tubes and centrifuged to separate the fibers from the supernatant. Total Fe mobilized into the supernatant was measured by the ferrozine and spectrophotometer method as described in Lund and Aust (1990) except in the case of desferrioxamine, in which the absorbance of the supernatant was measured directly in the spectrophotometer at 428 nm. The fibers were washed five times in deionized water to remove any remaining chelator solution, dried on an acid-washed watch glass at room conditions, and stored in glass vials with screw tops.

Scanning electron microscopy

The untreated fibers and those treated in the chelator-containing solutions for 30 d were examined with a Noran-Tracor Adem SEM equipped with a LaB_6 electron gun. Samples were dispersion mounted on C rounds and coated with approximately 100 Å of gold.

X-ray photoelectron spectroscopy

Near-surface composition and Fe oxidation state on the crocidolite samples were determined before and after the various solution treatments with a Perkin Elmer 5400 XPS (see Hochella, 1988, for a detailed description of XPS). Because all experiments were performed in triplicate, three independent sets of XPS data were collected for each experimental condition reported. Therefore, the XPS data reported in the Results section below are the averages of three measurements.

Each sample of crocidolite, in a matlike form, was mounted on a 1 in. diameter aluminum stub for examination. A colloidal C suspension (in isopropyl alcohol) was used as a mounting cement. Nonmonochromatic Al$K\alpha$ X-rays (1486.6 eV) were used to analyze a 3 mm^2 area on the mat of fibers. The Si 2p, Na 2s, Mg 2s, Fe 3p, and C 1s photolines were used for all analyses. These particular Si, Na, Mg, and Fe photolines were chosen because of their similar binding energies (and thus similar kinetic energies between 1370 and 1440 eV for Al$K\alpha$ X-rays). Using peaks with similar kinetic energies is important because the electrons that compose these peaks originate from a similar depth in the sample. The C 1s peak (kinetic energy $\approx$ 1176 eV) is the only core-level C peak that is attainable for analysis by XPS. The sources of C on the surface were the mounting cement and contamination from exposure to the solution and air.

A curve-fitting program (Labcalc) was used to determine the absolute area of the Na 2s and Fe 3p peaks (which have a slight overlap) and the $Fe^{2+}:Fe^{3+}$ ratio (Fig. 1). The Fe 3p line is best fit using three peaks, one rep-
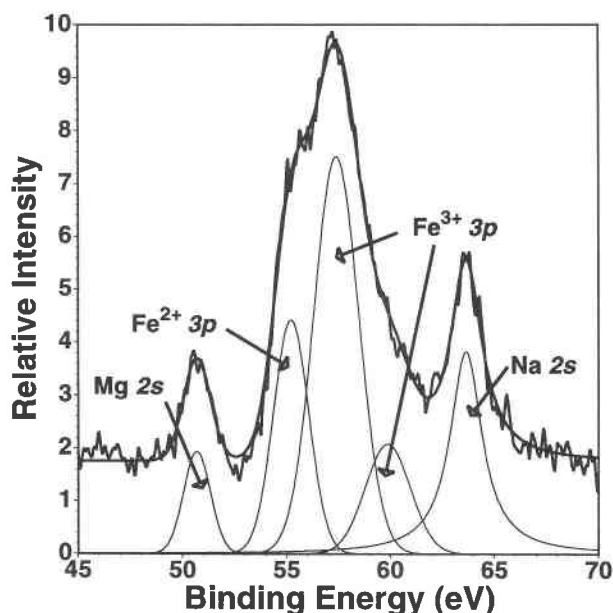
Fig. 1.   Example of a curve-fit XPS spectrum for Na 2s, Fe 3p, and Mg 2s photolines used in this study. The sum of all curves is superimposed on the actual spectrum. When determining the $Fe^{2+}:Fe^{3+}$ ratio, the Fe 3p line was fit using the three peaks shown following McIntyre and Zetaruk (1977). The relative positions of the three peaks were held constant, as were their widths and the relative intensities of the two Fe^{3+} lines. Only the relative intensities of the one Fe^{2+} line vs. the two Fe^{3+} lines were allowed to vary. The $Fe^{2+}:Fe^{3+}$ ratio is equal to the peak area ratio.
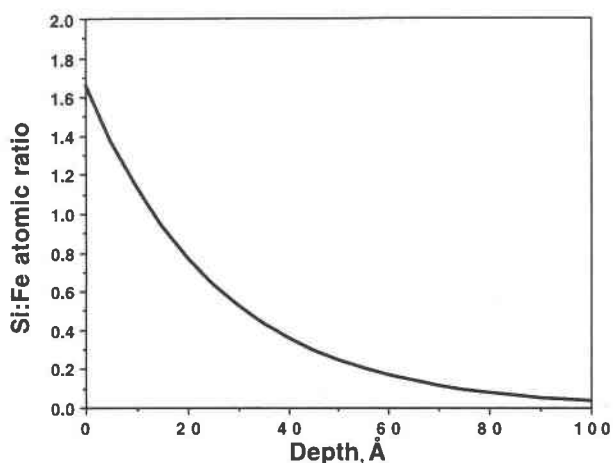
Fig. 2.   Theoretical change in Si:Fe ratio (as measured by XPS) as a function of Si leaching depth in angstroms. For example, at a hypothetical leaching depth of 0 Å (no leaching), Si:Fe = 1.65, the ratio of the untreated surface. The curve from this fixed point is derived from Eq. 7 using λ = 26 Å. As an example, an Si:Fe atomic ratio of 1.0, as measured by XPS, could result by leaching all Si in the near surface to a depth of approximately 13 Å.

resenting Fe^{2+} and two representing Fe^{3+}, following the often-cited example of McIntyre and Zetaruk (1977). The smaller of the two Fe^{3+} peaks is needed to account for the numerous multiplet-split peaks that appear on the high binding-energy side of the Fe 3p peak (Gupta and Sen, 1974). The area ratio of the Fe^{2+} fitted line relative to the two Fe^{3+} fitted lines is directly proportional to the $Fe^{2+}:Fe^{3+}$ ratio (Fig. 1).

The Fe^{2+}, Fe^{3+}, Na, Mg, and Si photolines were converted into semiquantitative compositional data using the following method. The number of atoms present in a given volume is related to the area under a photoline by the equation (Hochella, 1988)

$$I \propto n\sigma \qquad (5)$$

where I is the area under the peak, n is the atomic percentage in the measured volume of the sample, and σ is the photoionization cross section for the sampled orbital for the excitation energy used. The value of σ for each photoline was determined from the above equation using a value for n given by the bulk analysis reported above and a value for I from the XPS data of the untreated sample. Because the n values for Fe^{2+} and Fe^{3+} were determined from the same photoline, their respective σ values were set equal on the basis of the cross section derived using the total Fe 3p peak area and the Fe_{tot} content.

Using the calculated σ values and I from the XPS data, the actual values for n were determined for each cation in every sample. The n values for Fe_{tot}, Fe^{2+}, Fe^{3+}, Mg, and Na were then considered proportionately to Si. This cation to Si ratio was needed to compare the XPS data from sample to sample because the sampling volume analyzed in each experiment varies owing to exact sample mounting and instrument conditions. Although I for each photoline varies proportionally to the amount of sample analyzed, the cation to Si ratios for a given sample are independent of the analytic volume, allowing ratios to be compared between samples. The changes in cation to Si ratios were then used to follow the near surface composition of the mineral caused by reaction with the solutions.

To test quantitatively for the development of leached layers on the crocidolite surface within the 30 d length of the treatments, we evaluated the Na:Si, Mg:Si, and Fe:Si ratios as follows. The depth from which photoelectrons are derived depends on the attenuation length, λ, of the solid for an electron with the kinetic energy of interest (see Hochella, 1988). Attenuation length is formally defined as the distance at which the probability of an electron escaping from a solid without the occurrence of an inelastic scattering event drops to e^{-1}. Therefore, there is an exponential reduction in signal as a function of depth, which is represented by the equation

$$\% \text{ signal} = (1 - e^{-a}) \times 100 \qquad (6)$$

where a is the number of attenuation lengths. Therefore, 63% of the signal comes from above 1λ, 86% from above 2λ, and 95% from above 3λ (a = 1, 2, and 3, respectively). By convention, the 3λ level in the sample is called the analysis depth. For example, in amorphous SiO_2, λ for the Si 2p photoelectrons ejected by AlKα X-rays has been

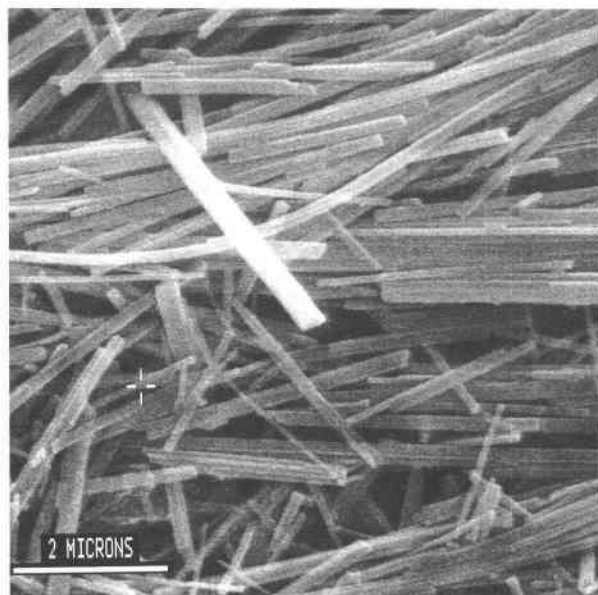Fig. 3. SEM photomicrograph of crocidolite reacted in the presence of citrate for 30 d.
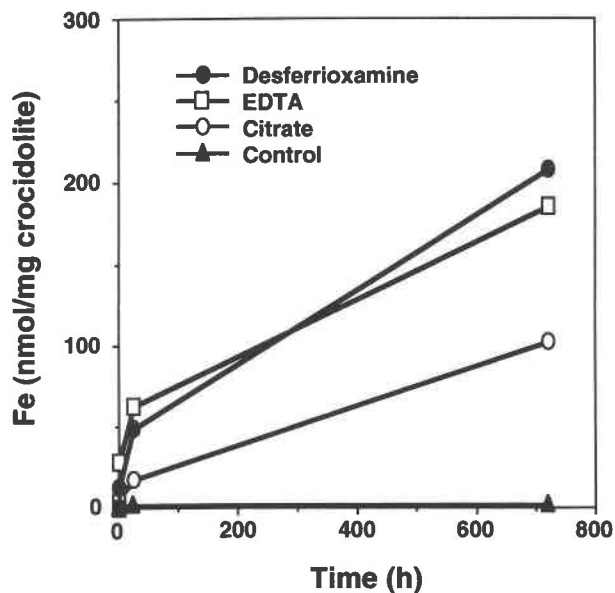

Fig. 4. Solution data showing nanomoles of Fe released into the supernatant per milligram of crocidolite. The durations of the experiments were 1, 24, and 720 h. Each point represents the average of three experiments. At 1 and 24 h, the sizes of the actual data points on the plot are larger than two standard deviations about the mean. At 720 h, the sizes of the data points are approximately one standard deviation about the mean.

measured to be 26 Å (Hochella and Carim, 1988), making the 3λ analysis depth 78 Å. Because all the photolines for the electrons being analyzed were chosen to have kinetic energies similar to Si 2p, the λ for these cations should be within a few angstroms of that for Si. Therefore, in this study one can calculate the depth of leaching of one element with respect to another in the near surface. For example, if the depth of leaching for a given cation with respect to Fe is equal to 1λ, one would expect the signal for that cation to be reduced by 63% relative to Fe (Fig. 2). Equation 6 is generalized to yield information about the depth of leaching in the following way:

$$\% \text{ signal reduction} = (1 - e^{-x/\lambda}) \times 100 \qquad (7)$$

where x is equal to the depth of cation leaching with respect to some other element. Thus, knowing the amount of cation signal reduction with respect to another element allows the depth of leaching relevant to that element pair to be determined as demonstrated graphically in Figure 2. We used this scheme to look for the possible leaching of Na, Mg, and Fe relative to Si, and Si relative to Fe.

The approach presented above assumes that the attenuation length is similar in the fresh material and the leached overlayer. This is probably a very good assumption because attenuation lengths are similar for oxides and silicates (Hochella, 1988). However, calculating apparent leaching depths in this way (or any other way) should still be considered only a qualitative measurement. As demonstrated by Hochella (1990), leaching depths are probably not uniform over a surface. Even if leaching depths were uniform, the analyzed surface would have to be flat for the approach presented above to be fully valid. Assuming that surface roughness and leaching

depth patterns are consistent for all crocidolite samples measured in this study, we can make best use of the calculated leach depths in a relative sense.

RESULTS

SEM imaging

Figure 3 is an SEM image of fibers that reacted in the presence of citrate for 30 d. This and other SEM images at higher magnification show no evidence of dissolution features or of a surface precipitate. Similar results were obtained for all fibers examined after reaction.

Solution analysis

The amount of Fe found in the posttreatment solutions is shown in Figure 4 as nanomoles of Fe in solution per milligram of treated sample. Even after 30 d, the Fe_{tot} released to solution in the control samples averaged only 1 nmol/mg. This amount of Fe, equivalent to 1 nmol/mL of solution in these experiments, is right at the detection limit of the ferrozine and spectrophotometer method used in this study. Therefore, Fe in solution for these experiments may actually be less. The introduction of chelators greatly increased the release of Fe from the crocidolite fibers. After 30 d, the amount of Fe released was roughly 200 nmol/mg from the EDTA- and desferrioxamine-treated fibers and approximately 100 nmol/mg from the citrate-treated fibers.
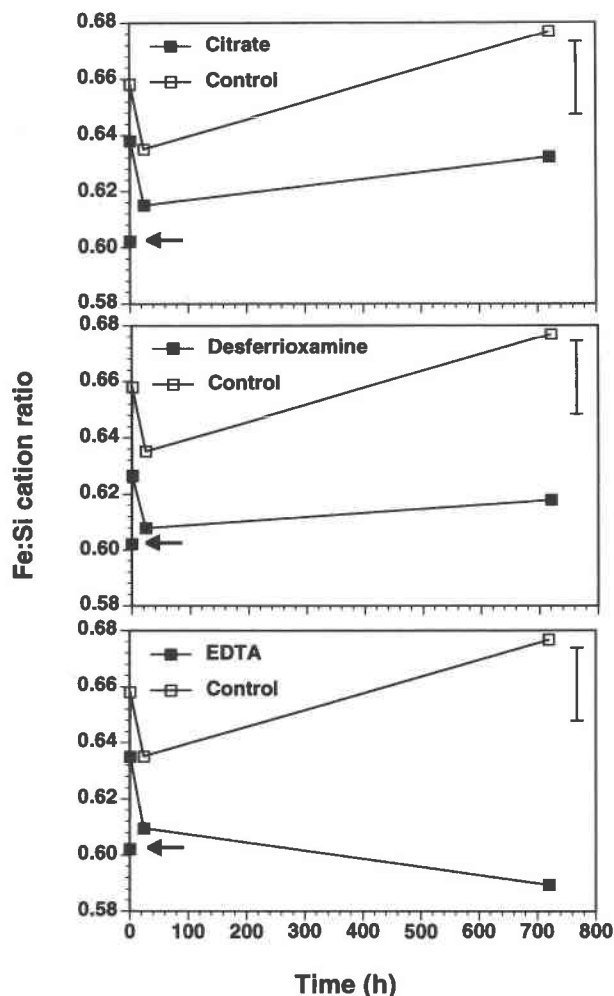
Fig. 5. Fe:Si cation ratios as determined by XPS for control and chelator experiments. Each point is the average of XPS data obtained from three identical experiments. Data points are plotted at 1, 24, and 720 h on the horizontal axis. The arrow on the left of each plot represents the starting elemental ratio of the untreated sample. The error bar on the right side of each plot represents one standard deviation as determined from triplicate experiments.

XPS analysis

Fe vs. Si surface analysis. The XPS data in Figure 5 show how the Fe:Si ratios for both the control and treated fibers changed over the 30 d period. All the chelator-exposed samples and the control group exhibited an initial rise of the Fe:Si ratio in the first hour and then a decrease of this ratio after 24 h. In the control experiment, this initial action was followed by an increase in the Fe:Si ratio after 30 d. The difference in the Fe:Si ratios between the untreated sample and the average of the 30 d control samples was significant (about three standard deviations). The desferrioxamine-, EDTA-, and citrate-treated samples showed slight variations in the Fe:Si ratio relative to the starting value after reacting in the solutions
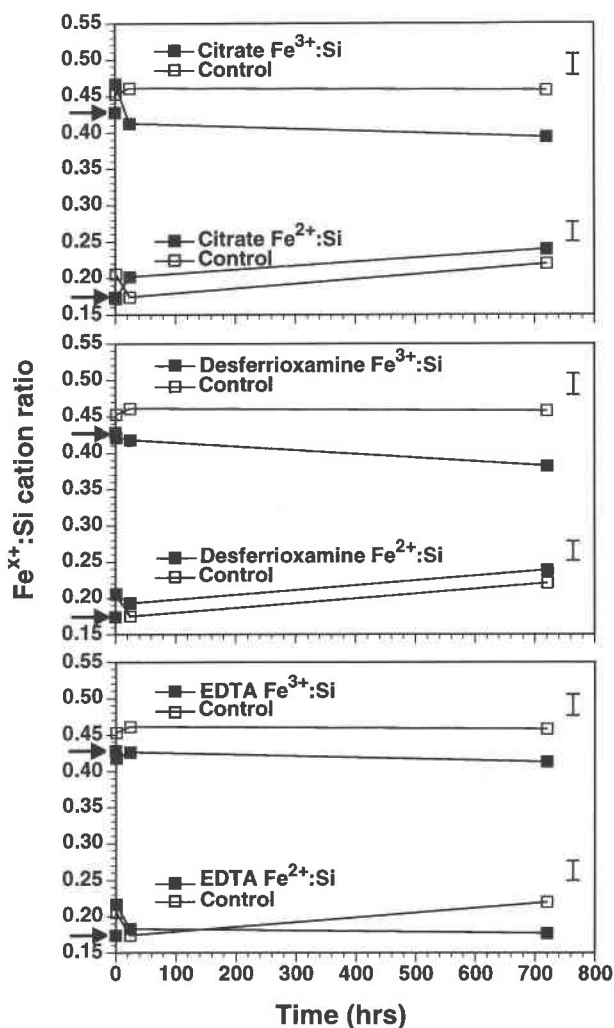

Fig. 6. Fe:Si cation ratios vs. time showing the Fe^{2+} and Fe^{3+} components. See the caption to Fig. 5 for more details.

for 30 d, but these changes were not more than one standard deviation. The Fe:Si ratio for the control was significantly higher than those ratios in the chelator groups after 30 d.

Data were also collected to determine how the surface Fe^{2+}:Si and Fe^{3+}:Si ratios changed with time (Fig. 6). The Fe^{3+}:Si ratio in the control increased initially in the first 24 h and then remained constant at about one standard deviation greater than the untreated sample. The citrate- and desferrioxamine-treated samples showed a decrease in the ratio of about one standard deviation after 30 d, and the EDTA-treated sample changed less than one standard deviation. The Fe^{3+}:Si ratio in the control was greater than that for the chelator groups by 1.5–2.5 standard deviations after 30 d.

The Fe^{2+}:Si ratio for the control rose slightly more than one standard deviation after 30 d. The Fe^{2+}:Si ratios also rose in the citrate- and desferrioxamine-treated samples by more than two standard deviations, whereas the

Fig. 7. Mg:Si cation ratios vs. time. See the caption to Fig. 5 for more details.
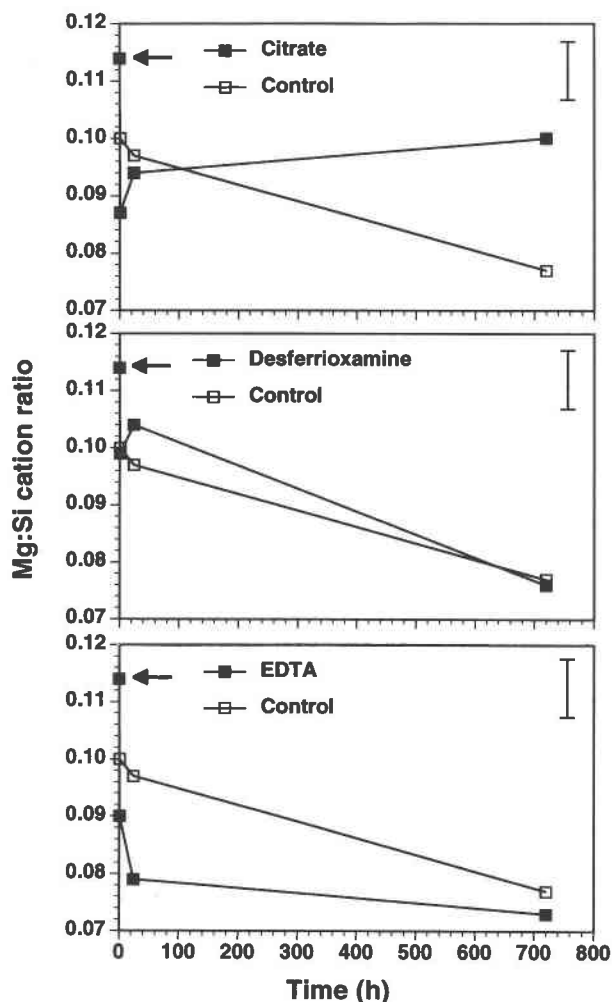
Fig. 8. Na:Si cation ratios vs. time. See the caption to Fig. 5 for more details.

EDTA-treated samples experienced essentially no apparent change in the ratio after 30 d. All three chelator groups had a statistically similar Fe^{2+}:Si ratio after 30 d relative to the control (within one standard deviation for desferrioxamine and citrate, less than two standard deviations for EDTA).

Mg and Na vs. Si surface analysis. The Mg:Si ratios are shown in Figure 7. After 30 d, the control, desferrioxamine, and EDTA groups had a large decrease (four standard deviations) in the Mg:Si ratio in comparison with the initial ratio. The citrate group also showed a reduction in the Mg:Si ratio but less than half as much as the control, desferrioxamine, and EDTA groups. The citrate group was the only chelator group with a significantly different Mg:Si ratio relative to the control after 30 d.

Figure 8 shows the changes in the Na:Si ratios. Only the desferrioxamine group showed a significant decrease in the Na:Si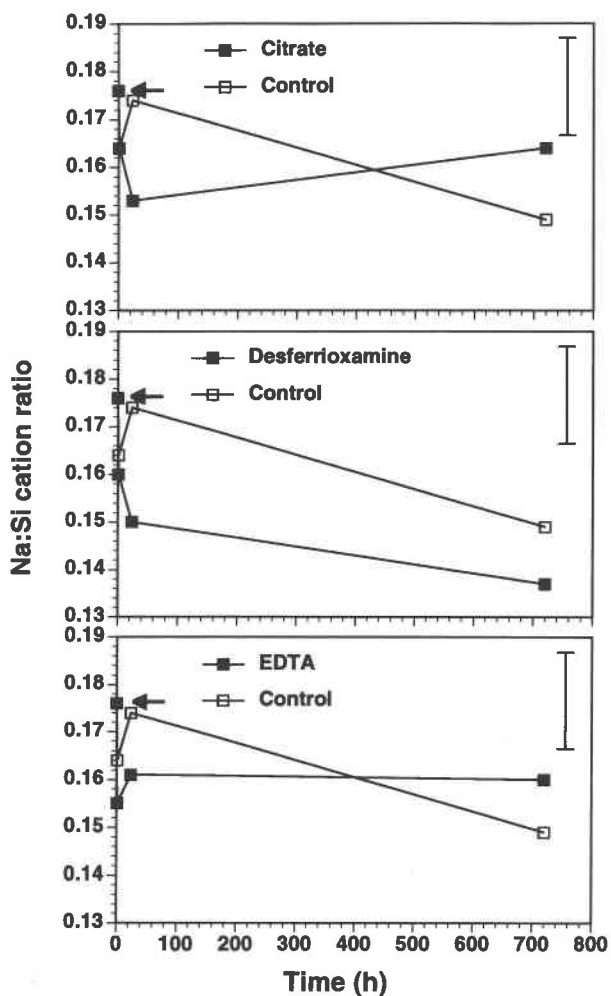 ratios after 30 d (two standard deviations), whereas the control (just over one standard deviation), citrate, and EDTA (less than one standard deviation) groups did not. In the case of all three chelator groups, the Na:Si ratio did not vary by more than one standard deviation from the control after 30 d.

C surface analysis. The C 1s spectra for all samples showed a relatively narrow, fully resolved peak to the low binding-energy side of an often complex, much broader band. The low binding-energy peak is clearly due to the colloidal C suspension used to cement the fibers to the sample stub (Hochella, 1988). The other portion of the C 1s spectra originated from the fibers. This band generally increased in width and complexity with the length of time of the treatment, irrespective of whether chelator was present in the experiment or not. This suggests that the C 1s signal from the fibers was not due to residual chelators on the surface after rinsing but to the progressive accumulation of adventitious C of various forms in aqueous solution, which has been seen before (Stipp and Hochella, 1991).

DISCUSSION

Control experiments

In the 30 d control experiments, the XPS data show a slight but significant increase in the Fe:Si ratio (equivalent to a Si:Fe ratio decrease for direct comparison with Fig. 2). This suggests the formation of a surface layer enriched in Fe with respect to Si. Using the leached layer thickness model and assumptions described in the Materials and Methods section, the thickness of the Si-depleted layer is calculated at about 5 Å, assuming the leached layer is completely depleted in Si but unchanged with respect to Fe (i.e., using Eq. 7; see Fig. 2). Although the data are consistent with such a depleted layer, other scenarios are possible. Si could be partially removed from the near surface, implying that the leached layer extends deeper into the mineral. Also, it is likely that the leaching depth is quite variable (Hochella, 1990). Nevertheless, the leached layer thickness model gives a relative sense of chemical variations at a surface and provides a convenient benchmark with which to compare other surfaces.

The Si-deficient layer suggested here could also reflect the precipitation of an iron oxide on the surface. Work by White and Yee (1985) on Fe oxidation and reduction in iron silicates shows that at near neutral pH, the rate of Fe^{3+} release is greatly decreased because of the initiation of ferric hydroxide or oxyhydroxide precipitation. However, we observed no increase in Fe^{3+} relative to either Si or Fe^{2+} according to the XPS data after 30 d (Fig. 6). Therefore, we conclude that precipitation of Fe^{3+}-containing phases was not responsible for the increase in the Fe:Si ratio in the control experiments. Also, although the bulk chemistry data show that the $Fe^{2+}:Fe^{3+}$ ratio ≈ 1 in the bulk mineral, the XPS data show an $Fe^{2+}:Fe^{3+}$ ratio of approximately 0.4 at the surface. This is probably the result of oxidation of the Fe at the surface long before any sample treatment. This surface abundance of nearly insoluble Fe^{3+} under these conditions (Baes and Mesmer, 1976) probably hinders Fe release at neutral pH but allows Si to be preferentially removed. Taken together, the above information suggests that the dissolution of crocidolite is dependent on the release of Fe, particularly Fe^{3+}, from the surface.

The XPS data for the control experiments also show a decrease in the Mg:Si and Na:Si ratios at 30 d that is equivalent to a 5 Å Na- and a 10 Å Mg-depleted layer with respect to Si. If Si were released from the surface, Na and Mg must have been leached as well but to a greater depth.

Because of the nature of a crocidolite fiber bundle, surface chemistry internal to the bundles (i.e., on the surfaces of fibrils accessible to solutions along grain boundaries) is probably an important component of the cell-mineral-fluid interaction. These surfaces would not be observable by classic surface-sensitive spectroscopies but would certainly contribute to changes in the solution chemistry, and reactions at these surfaces could possibly be studied directly with high-resolution transmission electron microscopy (HRTEM). Groups that have used HRTEM to study dissolution reactions and weathering processes internal to mineral grains include Ahn and Peacor (1987), Banfield and Eggleton (1988, 1990), and Banfield et al. (1991). Specifically for crocidolite, each fiber consists of exceptionally narrow (less than a few tenths of a micrometer in diameter) interlocking fibrils, as has been previously shown in TEM studies (e.g., Ahn and Buseck, 1991). Interfibril regions probably contain sheet silicates. The sheet silicates would be only minor to trace mineral components in a bulk sense, but they could be very influential in reactions with solutions (Veblen and Wylie, 1993).

Chelator experiments

As noted in the Results section, the $Fe^{2+}:Si$ and $Fe^{3+}:Si$ ratios for the 30 d EDTA, desferrioxamine, and citrate groups did not vary considerably from that of the untreated sample, but trends in the $Fe^{2+}:Si$ and $Fe^{3+}:Si$ ratios of at least the desferrioxamine and citrate groups appeared as though they would converge with time. This probably marks the beginning of the removal of the oxidized layer at the surface that was described in the previous section. As the outer oxidized layer is removed, the surface composition begins to approach that of the bulk, where $Fe^{2+}:Fe^{3+} \approx 1$, causing the $Fe^{2+}:Si$ and $Fe^{3+}:Si$ ratios to converge.

After 30 d in the presence of chelators, the total Fe:Si ratios did not significantly change. From this, one might infer that the crocidolite fibers dissolved congruently, i.e., Si was being released at a rate in stoichiometric proportion to Fe. Assuming that the complete dissolution of a fiber is a function of the release of Fe, Si, or both (i.e., this is the rate-limiting step), one can calculate an apparent fiber lifetime (see estimates below and accompanying assumptions). But it has been shown or inferred in other studies (e.g., Berner et al., 1985; Mogk and Locke, 1988; Hochella et al., 1988; Hellmann et al., 1990) that release-to-solution data and XPS observations generally do not have a simple correlation because the solution and XPS data measure two different things. The release-to-solution data give the total number of cations that have been liberated from the solid and have not participated in any kind of reprecipitation reaction. These data provide no information about where the cations originated. On the other hand, XPS data give the composition of the top several nanometers over a large area of the sample. XPS cannot detect what is happening on internal surfaces, and XPS data do not provide the distribution of cations within the depth of analysis (excluding angle-resolved XPS, which is not applicable on rough surfaces or fibers). Finally, the data cannot be used to determine leaching depth heterogeneity. Taken together, these limitations mean that release-to-solution data cannot be used to predict XPS results and vice versa. In fact, the same conclusion can be drawn from the data of a previous crocidolite dissolution study (Gronow, 1987). Results from this study show crocidolite dissolution to be incongruent according to so-

lution data after 1024 h between pHs of 4 and 9, yet XPS data show no change in the average surface chemistry at least over the first 50 h of reaction at pH 4. Further evidence of incongruent dissolution comes from Crawford (1980), an HRTEM study of crocidolite fibers before and after reaction with human blood serum in vitro or rodent lung tissue in vivo. About one-half of the fibers examined from both environments showed patchy (i.e., covering only portions of any one fiber), amorphous, presumably leached layers on the surface up to 100 Å thick. The other one-half of the fibers observed showed no dissolution rinds (i.e., the amphibole structure was seen extending all the way to the surface). This clearly demonstrates once again the heterogeneous nature of surface reactions (Hochella, 1990, 1993). Although the dissolution rinds were not chemically analyzed in the Crawford study, their composition probably varies from that of crocidolite (see Casey and Bunker, 1990, for an example of similar leached layers on feldspar grains that were chemically analyzed).

On the basis of these studies, we cannot say with full confidence from our experiments that Si is released in stoichiometric proportion to Fe even though the XPS data show that the Fe:Si ratios do not change from the untreated to the 30 d treated samples. However, we can say that the average composition of the top several tens of angstroms of these fibers maintains similar Fe:Si and Na:Si ratios over 30 d, that the surface becomes depleted in Mg, and that, at least for the desferrioxamine and citrate experiments, the average surface Fe oxidation state is reduced.

Fe:Si fluctuations in the first 24 h

The Fe:Si ratios determined from the XPS data for all the data groups showed an increase in the first hour followed by a decrease in the following hours up to the 24 h point. The reason for this consistent fluctuation is not known, but it may relate to highly reactive sites on the untreated fiber surface. The chelators probably do not play a role in this fluctuation because the same behavior is seen in the control group. We assume below that this fluctuation is not important in determining the long-term effects of chelators on crocidolite dissolution.

Fe-release lifetimes and implications for mineral-induced pathogenesis

Our goal in this part of the study was to estimate how long a crocidolite fiber can release Fe to surrounding solutions under the conditions used in this study. As discussed below, this has implications in understanding the biodurability of crocidolite fibers as well as their ability to induce lung disease.

The amount of Fe released into solution in the first day is not a good estimate of long-term Fe release because of the initial chemical fluctuations discussed above. To obtain a more reasonable Fe-release rate, the concentration change between the day 1 and day 30 data points for the control and each chelator group could be used. The use of 1 d as an appropriate starting point might be justified

by the crocidolite dissolution study of Gronow (1987); she showed that dissolution reaches an apparent steady state after this period of time. However, Chao and Aust (1994) showed that the Fe-release rate continues to slow after 30 d in desferrioxamine solutions for samples that were identical to those used in this study, but that the release rate between 30 and 90 d is relatively stable. During this 60 d period, approximately 140 nmol of Fe was released per milligram of fiber, equivalent to a loss of 2.7% of the total Fe present. At that rate, the fiber would be depleted in Fe (probably fully dissolved) in approximately 6 yr. Choa and Aust (1994) did not use citrate under the conditions of our experiments, but if the Fe release caused by citrate slowed proportionally with what was observed for desferrioxamine in this study, the Fe-release lifetime in a citrate solution under the conditions of our experiments would be approximately 13 yr.

Our estimates of Fe-release lifetimes of crocidolite fibers should be used in biodurability assessments with caution. In the lung, fibers may be engulfed in scavenging cells (phagocytes) and subjected to different chemistries (e.g., pH $\approx$ 4–4.5) compared with those of the fluids we used. This would almost certainly result in shorter lifetimes, as would increasing the ambient temperature (our experiment temperatures were ~15 °C lower than typical body temperatures). Further, Lund and Aust (1990) showed that the presence of ascorbate, which is found in physiological fluids, can increase the release rate of Fe^{2+} from crocidolite under conditions similar to those of the control and chelator experiments of this study. On the other hand, fibers in lungs also can be partially covered with crystalline Fe-rich coatings believed to be derived from proteins such as hemosiderin and ferritin (Pooley, 1972; Churg and Warnock, 1977). This could significantly slow the overall rate of Fe release from the fiber. Finally, many other agents in lung fluids that have not been tested may have significant effects on fiber surface chemistry and dissolution. Nevertheless, a recent study by Chao et al. (1994) has demonstrated that crocidolite fibers phagocytized by cultured human lung carcinoma cells show a similar Fe-release rate over the first 24 h as crocidolite incubated in citrate-bearing solutions similar to the ones used in this study. Unfortunately, longer duration studies of this type were not possible because of the simultaneous occurrence of cell death and replication, making unique interpretation of the data impossible.

The Fe-release lifetimes of crocidolite fibers discussed above correspond well with what is already known about the biodurability of asbestos minerals from lung-burden studies. Wagner et al. (1974) noted that rats continuously exposed to amphibole fibers suffered an ever increasing lung burden, whereas rats continuously exposed to chrysotile fibers showed only a moderate lung burden, which leveled off with time. Jones et al. (1989) more recently came to a similar conclusion. This fiber accumulation pattern in lung tissue has also been shown to be the same in humans (Churg, 1993, and references therein). These observations are consistent with Hume and Rimstidt

(1992), who studied the dissolution behavior of chrysotile fibers at a temperature and pH range consistent with human lung conditions. For these conditions, they estimated that a 1 μm diameter fiber of chrysotile would completely dissolve in <1 yr. Considering these studies, it is no surprise that the crocidolite burden recovered from autopsied human lungs is always considerably greater than the proportion of crocidolite fiber dust in the air source responsible for the lung contamination (e.g., Wagner et al., 1982; Gardner et al., 1986; Churg, 1988, 1993). Perhaps either chrysotile fibers are not making it into the lung through the upper bronchial tubes relative to the crocidolite fibers for mechanical or aerodynamic reasons, or crocidolite fibers are much more biodurable. However, Churg et al. (1984) showed unequivocally that chrysotile fibers can be found in both the peripheral and central portions of the human lung, indicating that the probable cause of these observations is greater biodurability of crocidolite fibers.

SUMMARY AND CONCLUSIONS

We observed with X-ray photoelectron spectroscopy, for the first time, the change in crocidolite surface chemistry in the presence of saline solutions containing chelators that partially mimic physiological fluids. Over 30 d, crocidolite fiber surfaces become depleted in Mg relative to Fe and Si. In addition, Fe is removed at a highly accelerated rate relative to Fe removal in the absence of the chelators, yet the ratio of Fe to Si on the surface of these fibers remains approximately the same. Although we cannot pronounce the dissolution mechanisms of these fibers from these data without more solution composition information, the data do suggest that the fibers dissolve relatively quickly under the influence of chelators, considering the insolubility of Fe in pH-neutral aqueous solutions. After rinsing the fibers briefly in deionized water after 30 d in the presence of chelators, no evidence was found of chelators remaining on the fiber surfaces, suggesting that they are only weakly bound to the dissolving surface, although their influence in fiber dissolution is dramatic. Despite this, estimates of Fe-release lifetimes under the conditions of these experiments is on the order of 10 yr. It is possible that crocidolite dissolution may provide a considerable and long-lasting source of Fe potentially available to promote DNA damage in lung tissue.

ACKNOWLEDGMENTS

REFERENCES CITED

Ahn, J.H., and Buseck, P.R. (1991) Microstructures and fiber-formation mechanisms of crocidolite asbestos. American Mineralogist, 76, 1467–1478.

Ahn, J.H., and Peacor, D.R. (1987) Kaolinitization of biotite: TEM data and implications for an alteration mechanism. American Mineralogist, 72, 353–356.

Aust, A.E., and Lund, L.G. (1990) The role of iron in asbestos-catalyzed damage to lipids and DNA. Biological Oxidation Systems, 2, 597–605.

——— (1991) Iron mobilization from crocidolite results in enhanced iron-catalyzed oxygen consumption and hydroxyl radical generation in the presence of cysteine. In R.C. Brown, J.A. Hoskins, and N.F. Johnson, Eds., Mechanisms in fibre carcinogenesis, p. 397–405. NATO ASI Series, Plenum, New York.

Baes, C.F., Jr., and Mesmer, R.E. (1976) The hydrolysis of cations, 489 p. Wiley, New York.

Banfield, J.F., and Eggleton, R.A. (1988) Transmission electron microscope study of biotite weathering. Clays and Clay Minerals, 36, 47–60.

——— (1990) Analytical transmission electron microscope studies of plagioclase, muscovite, and K-feldspar weathering. Clays and Clay Minerals, 38, 77–89.

Banfield, J.F., Jones, B.F., and Veblen, D.R. (1991) An AEM-TEM study of weathering and diagenesis, Abert Lake, Oregon: I. Weathering reactions in the volcanics. Geochimica et Cosmochimica Acta, 55, 2781–2793.

Berner, R.A., Holdren, G.R., Jr., and Schott, J. (1985) Surface layers on dissolving silicates. Geochimica et Cosmochimica Acta, 43, 1173–1186.

Brown, R.C., Carthew, P., Hoskins, J.A., Sara, E., and Simpson, C.F. (1990) Surface modification can affect the carcinogenicity of asbestos. Carcinogenesis, 11, 1883–1885.

Campbell, W.J., Huggins, C.W., and Wylie, A.G. (1980) Bureau of mines report of investigations no. 8452.

Casey, W.H., and Bunker, B. (1990) Leaching of mineral and glass surfaces during dissolution. In Mineralogical Society of America Reviews in Mineralogy, 23, 397–426.

Chao, C., and Aust, A.E. (1993) Photochemical reduction of ferric iron by chelators results in DNA strand breaks. Archives of Biochemistry and Biophysics, 300, 544–550.

——— (1994) Effect of long-term removal of iron from asbestos by desferrioxamine B on subsequent mobilization by other chelators and induction of DNA single-strand breaks. Archives of Biochemistry and Biophysics, 308, 64–69.

Chao, C., Lund, L.G., Zinn, K.R., and Aust, A.E. (1994) Iron mobilization from crocidolite asbestos by human lung carcinoma cells. Archives of Biochemistry and Biophysics, 314, 384–391.

Churg, A. (1988) Chrysotile, tremolite, and mesothelioma in man. Chest, 93, 621–628.

——— (1993) Asbestos lung burden and disease patterns in man. In Mineralogical Society of America Reviews in Mineralogy, 28, 410–426.

Churg, A., and Warnock, M.L. (1977) Analysis of the cores of ferruginous (asbestos) bodies from the general population. Laboratory Investigations, 37, 280–286.

Churg, A., DePaoli, L., Kempe, B., and Stevens, B. (1984) Lung asbestos content in chrysotile workers with mesothelioma. American Reviews on Respiratory Disease, 130, 1042–1045.

Craighead, J.E., Abraham, J.L., Churg, A., Green, F.H.Y., Kleinerman, J., Pratt, P.C., Seemayer, T.A., Vallaythan, V., and Weill, H. (1982) The pathology of asbestos-associated diseases of the lungs and pleural cavities: Diagnostic criteria and proposed grading scema. Archives of Pathology and Laboratory Medicine, 106, 544–596.

Crawford, D. (1980) Electron microscopy applied to studies of the biological significance of defects in crocidolite asbestos. Journal of Microscopy, 120, 181–192.

Eborn, S.K., and Aust, A.E. (1995) Effect of iron aquisition on induction of DNA single-strand breaks by erionite, a carcinogenic mineral fiber. Archives of Biochemistry and Biophysics, 316, 507–514.

Gardner, M.J., Winter, P.E., Pannett, B., and Powell, C.A. (1986) Follow up study of workers manufacturing chrysotile asbestos cement products. British Journal of Industrial Medicine, 43, 726.

Ghio, A.J., Kennedy, T.P., Stonehuerner, J.G., Crumbliss, A.L., and Hoidal, J.R. (1994) DNA strand breaks following in vitro exposures to asbestos increases with surface-complexed $[Fe^{3+}]$. Archives of Biochemistry and Biophysics, 311, 13–18.

Goodglick, L.A., and Kane, A.B. (1986) Role of reactive oxygen metabolites in crocidolite asbestos toxicity to mouse macrophages. Cancer Research, 46, 5558–5566.

Gronow, J.G. (1987) The dissolution of asbestos fibers in water. Clay Minerals, 22, 21–35.

Gulumian, M., van Wyk, J.A., Hearne, G.R., Kolk, B., and Pollak, H. (1993) ESR and Mössbauer studies on detoxified crocidolite: Mechanism of reduced toxicity. Journal of Inorganic Biochemistry, 50, 133–143.

Gupta, R.P., and Sen, S.K. (1974) Calculation of multiplet structure of core p-vacancy levels. Physical Review B, 10, 71–77.

Guthrie, G.D., Jr., and Mossman, B.T. (1993) Merging the geological and biological sciences: An intergrated approach to the study of mineral-induced pulmonary diseases. In Mineralogical Society of America Reviews in Mineralogy, 28, 1–5.

Hardy, J.A., and Aust, A.E. (1995) Iron in asbestos chemistry and carcinogenicity. Chemical Reviews, 95, 97–118.

Hart, R.W., Kendig, O., Blakeslee, J., and Mizuhira, V. (1980) Effect of cellular ingestion on the elemental ratio of asbestos. In R.C. Brown, M. Chamberlain, R. Davies, and I.P. Gormley, Eds., The in vitro effects of mineral dusts, p. 191–199. Academic, London.

Hellmann, R., Eggleston, C.M., Hochella, M.F., Jr., and Crerar, D.A. (1990) The formation of leached layers on albite surfaces during dissolution under hydrothermal conditions. Geochimica et Cosmochimica Acta, 54, 1267–1281.

Hering, J.G., and Stumm, W. (1990) Oxidative and reductive dissolution of minerals. In Mineralogical Society of America Reviews in Mineralogy, 23, 427–465.

Hochella, M.F., Jr. (1988) Auger electron and X-ray photoelectron spectroscopies. In Mineralogical Society of America Reviews in Mineralogy, 18, 573–638.

——— (1990) Atomic structure, microtopography, composition, and reactivity of mineral surfaces. In Mineralogical Society of America Reviews in Mineralogy, 23, 87–132.

——— (1993) Surface chemistry, structure, and reactivity of hazardous mineral dust. In Mineralogical Society of America Reviews in Mineralogy, 28, 275–308.

Hochella, M.F., Jr., and Carim, A.H. (1988) A reassessment of electron escape depths in silicon and thermally grown silicon dioxide thin films. Surface Science, 197, L260–L268.

Hochella, M.F., Jr., Ponader, H.B., Turner, A.M., and Harris, D.W. (1988) The complexity of mineral dissolution as viewed by high resolution scanning Auger microscopy: Labradorite under hydrothermal conditions. Geochimica et Cosmochimica Acta, 52, 385–394.

Hume, L.A., and Rimstidt, J.D. (1992) The biodurability of chrysotile asbestos. American Mineralogist, 77, 1125–1128.

Jaurand, M.C., Bignon, J., Sebastien, P., and Goni, J. (1977) Leaching of chrysotile asbestos in human lungs. Environmental Research, 14, 245–254.

Jones, A.D., Vincent, J.H., McIntosh, C., McMillan, C.H., and Addison, J. (1989) The effect of fiber durability on the hazard potential of inhaled chrysotile asbestos fibers. Experimental Pathology, 37, 98–102.

Kamp, D.W., Graceffa, P., Pryor, W.A., and Weitzman, S.A. (1992) The role of free radicals in asbestos-induced diseases. Free Radical Biology and Medicine, 12, 293–315.

Kennedy, T.P., Dodson, R., Rao, N.V., Ky, H., Hopkins, C., Baser, M., Tolley, E., and Hoidal, J.R. (1989) Dusts causing pneumoconiosis generate ·OH and produce hemolysis by acting as Fenton catalysts. Archives of Biochemistry and Biophysics, 269, 359–364.

Klockars, M., Hedenborg, M., and Vanhala, E. (1990) Effect of two particle surface-modifying agents, polyvinylpyridine-N-oxide and carbomethylcellulose, on the quartz and asbestos mineral fiber-induced production of reactive oxygen metabolites by human polymorphonuclear leukocytes. Archives of Environmental Health, 45, 8–14.

Lehnert, B.E. (1993) Defense mechanisms against inhaled particles and associated particle-cell interactions. In Mineralogical Society of America Reviews in Mineralogy, 28, 427–469.

Lund, L.G., and Aust, A.E. (1990) Iron mobilization from asbestos by chelators and ascorbic acid. Archives of Biochemistry and Biophysics, 278, 60–64.

——— (1992) Iron mobilization from crocidolite asbestos greatly enhances crocidolite-dependent formation of DNA single-strand breaks in ϕX174 RFI DNA. Carcinogenesis, 13, 637–642.

Lund, L.G., Williams, M.G., Dodson, R.F., and Aust, A.E. (1994) Iron associated with asbestos bodies is responsible for the formation of single strand breaks in ϕX174 RFI DNA. Occupational and Environmental Medicine, 51, 200–204.

Martell, A.E., and Smith, R.M. (1974) Critical stability constants, vol. 1, 470 p. Plenum, New York.

——— (1977) Critical stability constants, vol. 3, 496 p. Plenum, New York.

McDonald, J.C. (1990) Cancer risks due to asbestos and man-made fibres. Recent Results in Cancer Research, 120, 122–133.

McDonald, J.C., and McDonald, A.D. (1986a) Epidemiology of malignant mesothelioma. In K. Antman and J. Aisner, Eds., Asbestos related malignancy, p. 57–79. Grune and Stratton, New York.

——— (1986b) Epidemiology of asbestos-related lung cancer. In K. Antman and J. Aisner, Eds., Asbestos related malignancy, p. 31–56. Grune and Stratton, New York.

McIntyre, N.S., and Zetaruk, D.G. (1977) X-ray photoelectron spectroscopic studies of iron oxides. Analytical Chemistry, 49, 1521–1529.

Mogk, D.W., and Locke, W.W., III (1988) Application of auger electron spectroscopy (AES) to naturally weathered hornblende. Geochimica et Cosmochimica Acta, 52, 2537–2542.

Morgan, A., Holmes, A., and Gold, C. (1971) Studies of the solubility of constituents of chrysotile asbestos in vivo using radioactive tracer techniques. Environmental Research, 4, 558–570.

Nolan, R.P., and Langer, A.M. (1993) Limitations of the Stanton hypothesis. In Mineralogical Society of America Reviews in Mineralogy, 28, 308–326.

Pooley, F.D. (1972) Asbestos bodies, their formation, composition and character. Environmental Research, 5, 363–379.

Schindler, P.W. (1990) Co-adsorption of metal ions and organic ligands: Formation of ternary surface complexes. In Mineralogical Society of America Reviews in Mineralogy, 23, 281–307.

Stanton, M.F., Layard, M., Tegeris, A., Miller, E., May, M., Morgan, E., and Smith, A. (1981) Relation of particle dimension to carcinogenicity of amphibole asbestoses and other fibrous minerals. Journal of the National Cancer Institute, 67, 965–975.

Stipp, S.L., and Hochella, M.F., Jr. (1991) Structure and bonding environment at the calcite surface as observed with X-ray photoelectron spectroscopy (XPS) and low energy electron diffraction (LEED). Geochimica et Cosmochimica Acta, 55, 1723–1736.

Stumm, W. (1992) Chemistry of the solid-water interface, 428 p. Wiley, New York.

Veblen, D.R., and Wylie, A.G. (1993) Mineralogy of amphiboles and 1:1 layer silicates. In Mineralogical Society of America Reviews in Mineralogy, 28, 61–137.

Vu, V.T. (1993) Regulatory approaches to reduce human health risks associated with exposures to mineral fibers. In Mineralogical Society of America Reviews in Mineralogy, 28, 545–554.

Wagner, J.C. (1991) The discovery of the association between blue asbestos and mesotheliomas and the aftermath. British Journal of Industrial Medicine, 48, 399–403.

Wagner, J.C., Sleggs, C.A., and Marchand, P. (1960) Diffuse pleural mesotheliomas and asbestos exposure in the north western Cape Province. British Journal of Industrial Medicine, 17, 260–271.

Wagner, J.C., Berry, G., Skidmore, J.W., and Timbrell, V. (1974) The effects of the inhalation of asbestos in rats. British Journal of Cancer, 29, 252–269.

Wagner, J.C., Berry, G., and Pooley, F.D. (1982) Mesotheliomas and asbestos type in asbestos textile workers: A study of lung contents. British Medical Journal, 285, 603.

Weitzman, S.A., and Graceffa, P. (1984) Asbestos catalyzes hydroxyl and superoxide radical generation from hydrogen peroxide. Archives of Biochemistry and Biophysics, 228, 373–376.

White, A.F., and Yee, A. (1985) Aqueous oxidation-reduction kinetics associated with coupled electron-cation transfer from iron-containing silicates at 25°C. Geochimica et Cosmochimica Acta, 49, 1263–1275.

Zalma, R., Bonneau, L., Guignard, J., and Pezerat, H. (1987a) Formation of oxy radicals by oxygen reduction arising from the surface activity of asbestos. Canadian Journal of Chemistry, 65, 2338–2341.

——— (1987b) Production of hydroxyl radicals by iron solid compounds. Toxicology and Environmental Chemistry, 13, 171–187.